

Tunable anisotropic superfluidity in an optical kagome superlattice

Xue-Feng Zhang,¹ Tao Wang,^{1,2} Sebastian Eggert,¹ and Axel Pelster^{1,*}

¹Physics Department and Research Center OPTIMAS,

Technical University of Kaiserslautern, 67663 Kaiserslautern, Germany

²Department of Physics, Harbin Institute of Technology, Harbin 150001, China

We study the phase diagram of the Bose-Hubbard model on the kagome lattice with a broken sublattice symmetry. Such a superlattice structure can naturally be created and tuned by changing the potential offset of one sublattice in the optical generation of the frustrated lattice. The superstructure gives rise to a rich quantum phase diagram, which is analyzed by combining Quantum Monte Carlo simulations with the Generalized Effective Potential Landau Theory. Mott phases with non-integer filling and a characteristic order along stripes are found, which show a transition to a superfluid phase with an *anisotropic* superfluid density. Surprisingly, the direction of the superfluid anisotropy is changing between different symmetry directions as a function of the particle number or the hopping strength. Finally, we discuss characteristic signatures of anisotropic phases in time-of-flight absorption measurements.

PACS numbers: 05.30.Jp,75.40.Mg,78.67.Pt

Ultracold atoms in optical lattices are prominently used to simulate many-body systems in condensed matter physics [1–5]. One of the most striking experiments is the Mott insulator–superfluid quantum phase transition of ultracold bosons in optical lattice built with counter-propagating lasers [6]. It can be described by the seminal Bose-Hubbard model [7, 8], where each parameter is precisely adjustable in the experiment. With the rapid advances in experimental techniques [9] the many-body physics can now be analyzed on more complex lattice geometries. On the one hand, the lattice symmetry can be reduced by adding additional lasers or tuning their relative strength, leading to a superlattice structure [10–13], which can give rise to insulator phases with fractional fillings [14–18]. On the other hand, it is also possible to *enhance* the residual entropy of the many-body system by using frustrated lattices, which have recently been realized using sophisticated optical techniques [19–21].

Theoretically, many interesting phases have been predicted in frustrated lattices such as spin-liquids [22–28], valence bond solids [29], string excitations [30], ordered metals [31], chiral fractional edge states [32], and super-solids [33–36]. Unfortunately, however, in all these scenarios longer range interactions beyond the on-site Bose-Hubbard model are assumed, which require dipolar interactions and are experimentally much harder to handle. On the other hand, the intriguing interplay between a superlattice and the kagome lattice has never been explored before for the on-site Bose-Hubbard model. This is surprising since a superlattice structure can be created naturally in optically generated kagome lattices, and insulating phases with fractional filling occur without the need of longer range interaction as discussed below. We now analyze the detailed phase diagram of the Bose-Hubbard model on the kagome lattice with a tunable superlattice structure. In addition to the fractionally filled ordered phases in the quantum phase diagram, the most striking

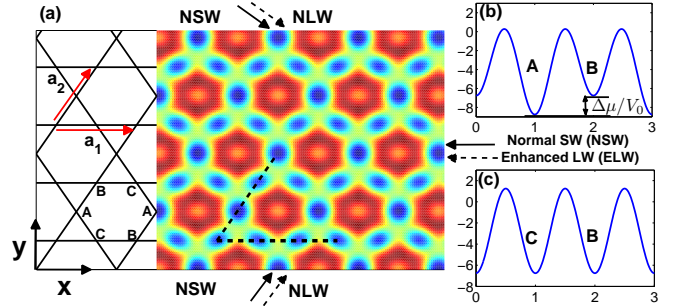


FIG. 1: (a) Potential from Eq. (1) of the optical kagome superlattice using an enhanced LW laser in the x -direction with $\gamma = 1.5$. Potential along cuts (dashed lines) in the b) a_2 -direction and c) a_1 -direction, respectively, showing the resulting potential offset $\Delta\mu$ for sublattice A.

features are found in the unusual properties of the Bose condensed phase, where the anisotropic superfluid density spontaneously picks a preferred direction depending on filling and interaction. This leads to a characteristic signature in time-of-flight experiments.

Let us first consider the optical generation of a kagome lattice, which recently has been achieved in experiment by using standing waves from a long wavelength 1064 nm (LW) laser and from a short wavelength 532 nm (SW) laser, which are counterpropagating from three 120° directions [21]. The superposition of the corresponding two triangular lattices results in a kagome lattice if the laser strengths are exactly equal from all directions. Any slight variation of this setup results in a superlattice structure, which of course can in turn be used as an additional tunable parameter. For example, enhancing the potential from the LW laser in the x -direction by a factor $\gamma = V_E/V_0 > 1$ results in a combined optical potential

$$V_c/V_0 = \gamma^2 - 1 + 4\gamma \cos(\sqrt{3}kx) \cos(ky) + 2 \cos(2ky)$$

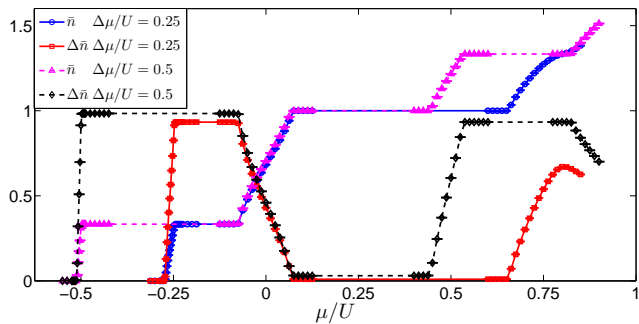


FIG. 2: Average density $\bar{n} = (n_A + n_B + n_C)/3$ and density difference $\Delta n = n_A - (n_B + n_C)/2$ versus μ from QMC with $T = U/300$ and $N = 243$ sites at $t/U = 0.025$ for different offsets $\Delta\mu/U$.

$$-2 \cos(4ky) - 4 \cos(2\sqrt{3}kx) \cos(2ky), \quad (1)$$

where $k = \sqrt{3}\pi/2\lambda_{\text{LW}}$ in units of the longer wavelength $\lambda_{\text{LW}} = 1064\text{nm}$. As depicted in Fig. 1 this potential leads to an offset of $\Delta\mu = 4(\gamma - 1)V_0 > 0$ on one of the sublattices A. Note, however, that this offset preserves the parity symmetry along the x - and the y -direction and does not increase the unit cell of the kagome lattice, which contains three sites.

Interacting bosons on this lattice can be represented by Wannier states, which leads to the well-known Bose-Hubbard model for the description of the lowest band in second quantized language

$$H = -t \sum_{\langle i,j \rangle} (\hat{a}_i^\dagger \hat{a}_j + \hat{a}_i \hat{a}_j^\dagger) + \frac{U}{2} \sum_i \hat{n}_i (\hat{n}_i - 1) - \mu \sum_i \hat{n}_i - \Delta\mu \sum_{i \in A} \hat{n}_i. \quad (2)$$

where the nearest-neighbor hopping amplitude t and the onsite interaction U are tunable parameters, which depend on the scattering cross-section and the potential depth V_0 [4]. In principle, the potential shift $\Delta\mu$ also affects the Wannier states and hence other parameters in Eq. (2), but for reasonably small values of $\Delta\mu$ these higher order corrections can be neglected since they preserve the symmetry of the problem. The chemical potential μ is used to tune the particle number in the grand-canonical ensemble. In the following we will use the stochastic cluster series expansion algorithm [37–39] for unbiased quantum Monte Carlo (QMC) simulations of this model. In addition the Generalized Effective Potential Landau Theory (GEPLT) provides an analytic method to estimate the phase boundaries in an expansion of the hopping parameter t/U [18, 40].

For vanishing hopping amplitude t in the atomic limit, the competition between U and $\Delta\mu$ can induce several incompressible insulating phases. When μ is less than $-\Delta\mu$, no site is occupied, and the Mott-0 phase is the energetically favored state. For a larger chemical potential

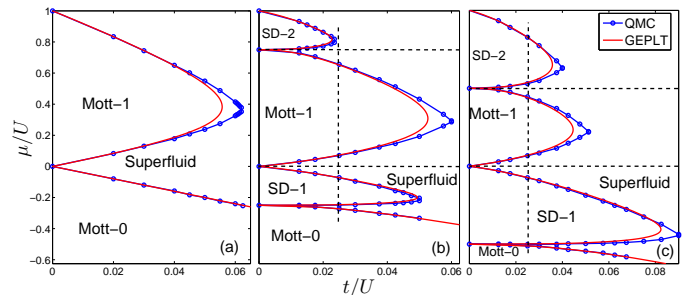


FIG. 3: Quantum phase diagram extrapolated to the thermodynamic limit obtained from QMC (blue) and multi-component GEPLT in second order in t/U (red) at (a) $\Delta\mu/U = 0$, (b) $\Delta\mu/U = 0.25$, and (c) $\Delta\mu/U = 0.5$. The vertical lines indicate the parameter ranges in Figs. 2 and 4 while the horizontal lines are used in Fig. 5

$-\Delta\mu < \mu < 0$, only sublattice A will be occupied with one boson per site while the other sites remain empty. This phase is therefore $1/3$ filled with an order in the form of occupied horizontal stripes. Such a $1/3$ striped density phase (SD) can also occur spontaneously in the extended Hubbard model when nearest and next-nearest interactions are included [32]. However, longer range interactions are notoriously difficult in optical lattices, so that the proposed superlattice is a convenient tool to study this phase. For positive values of $\mu > 0$, the system enters the familiar uniform Mott-1 insulator with filling factor one. Continuing this analysis for larger μ , we deduce that SD- n phases with fractional filling factor $n - 2/3$ occur for $U(n - 1) - \Delta\mu < \mu < U(n - 1)$, which are separated by Mott- n insulators with integer filling n for $U(n - 1) < \mu < Un - \Delta\mu$.

Both the integer filled Mott- n phases and the fractional SD- n phases remain stable for small finite hopping t . As shown in Fig. 2 for $t = 0.025 U$ there are plateaus of the average density $\bar{n} = (n_A + n_B + n_C)/3$ as a function of chemical potential, which are characteristic of those incompressible phases. In the fractionally filled SD- n phases the density difference $\Delta n = n_A - (n_B + n_C)/2$ between the sublattices shows plateaus with a value that is slightly reduced from unity due to virtual quantum excitations. The plateau states are separated by compressible phases, which are characterized by a finite superfluid density, i.e. an off-diagonal order with a spontaneously broken $U(1)$ gauge symmetry which will be analyzed in more detail below.

The corresponding phase diagram is mapped out in Fig. 3 using large scale QMC simulations. The second order GEPLT approximation is much less demanding and agrees quite well with the QMC data, except near the tips of the Mott lobes. With increasing offset $\Delta\mu$ the fractionally filled SD phases extend over a larger range not only in the chemical potential μ but also in the hopping t . In fact, the SD-1 phase for $\Delta\mu = 0.5 U$ is remarkably

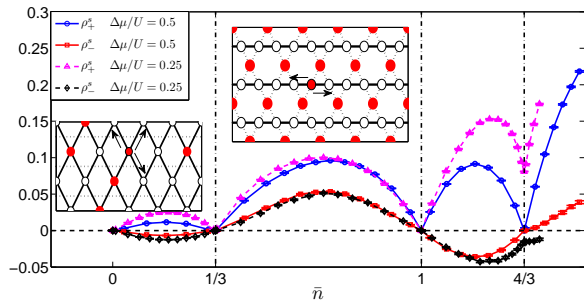


FIG. 4: Total superfluid density $\rho_+^s = (\rho_1^s + \rho_2^s)/2$ and superfluid density difference $\rho_-^s = \rho_1^s - \rho_2^s$ versus filling \bar{n} from QMC for $\beta U = 1200$ and $N = 243$ at $t/U = 0.025$. Inset: schematic illustration of the different mechanisms for positive and negative anisotropy parameters.

stable up to larger values of hopping t than the uniform Mott-1 phase. The transitions to the superfluid phase are always of second order and can be understood in terms of additional condensed particles (holes) on top of the Mott states as the chemical potential is increased (decreased).

One interesting detail in the phase diagram in Fig. 3 is the drastic dependence on $\Delta\mu$ of the shape of the Mott-0 phase transition line in the limit of small hopping, which changes from linear behavior $\mu(t) = -4t$ for $\Delta\mu = 0$ to quadratic behavior $\mu(t) = -\Delta\mu - 8t^2/\Delta\mu$ for large $\Delta\mu$. The linear dependence for $\Delta\mu = 0$ can be understood from a competition of chemical potential with the kinetic energy, analogously to the quantum melting on the triangular lattice [33]. For finite $\Delta\mu$, on the other hand, the melting of the Mott-0 phase takes place by additional particles on the sublattice A only, which is not connected by any first-order hopping processes. In the limit of small t , the kinetic energy of those particles is therefore determined by the second order hopping coefficient $\tilde{t} = t^2/\Delta\mu$, which explains the quadratic behavior of the phase boundary. The exact shape of the Mott-0 transition $\mu = -\Delta\mu/2 - t - \sqrt{\Delta\mu^2 - 4t\Delta\mu + 36t^2}/2$ can be determined from the single particle energy on the superlattice.

We now turn to the analysis of the order parameter in the superfluid phase. In the QMC simulations we determine the superfluid density along the lattice vector direction $\vec{a}_1 = (1, 0)$ using the winding number $\rho_1^s = \langle W_1^2 \rangle / 4\beta t$ and analogous for ρ_2^s along the lattice direction $\vec{a}_2 = (1, \sqrt{3})/2$ [41]. We use a system with $N = 243$ sites and periodic boundary conditions with $L = 9$ unit cells in both the \vec{a}_1 and \vec{a}_2 directions, which ensures that $\rho_1^s = \rho_2^s$ for the perfect kagome lattice. Note, that in general the superfluid density is a response tensor with four elements $\rho_{xx}^s, \rho_{xy}^s, \rho_{yx}^s, \rho_{yy}^s$ in the x - y -coordinate system [42]. Due to reflection symmetry the off-diagonal elements $\rho_{xy}^s = \rho_{yx}^s = 0$ must vanish. The relation to the superfluid densities along the lattice vectors

is given by $\rho_1^s = \rho_{xx}^s$ and $\rho_2^s = (\rho_{xx}^s + 3\rho_{yy}^s)/4$.

In order to analyze a possible anisotropy we consider the average superfluid density $\rho_+^s = (\rho_1^s + \rho_2^s)/2$ and the difference $\rho_-^s = \rho_1^s - \rho_2^s$ between the two lattice vector directions in Fig. 4 as a function of filling \bar{n} . For finite offsets $\Delta\mu = 0.25U$ and $\Delta\mu = 0.5U$ the superfluid density is indeed anisotropic, but surprisingly also changes the preferred direction with increasing filling \bar{n} . For low densities just above the Mott-0 phase the superfluid density is dominated by virtual hopping processes between the A sublattice. As illustrated in the left inset of Fig. 4 this virtual hopping process is not possible along the lattice vector \vec{a}_1 , which leads to an anisotropic superfluid density with $\rho_1^s < \rho_2^s$.

When the filling reaches $\bar{n} = 1/3$ the superfluid density drops to zero in the SD-1 phase as expected, but then shows the opposite anisotropy $\rho_1^s > \rho_2^s$ for $\bar{n} > 1/3$, which signals a different mechanism: At $\bar{n} = 1/3$ the A sublattice is completely filled, so that for slightly larger densities $\bar{n} > 1/3$ excess particles on the B and C sublattices are now responsible for the superfluid density. As shown in the right inset of Fig. 4, the B and C sublattices correspond to connected chains along the \vec{a}_1 direction, which are disconnected by occupied A sites. This immediately explains why $\rho_1^s > \rho_2^s$ in this case.

According to this analysis, positive anisotropies $\rho_-^s > 0$ are therefore a hallmark of an off-diagonal U(1) order parameter coexisting with a striped density order of a filled sublattice A. This situation is reminiscent of a supersolid where a stable density order exists on one filled sublattice and excess particles contribute to the superfluidity [33], with the main difference that in supersolids both the U(1) symmetry and the translational symmetry are *spontaneously* broken. Normally supersolid phases require longer range interactions beyond on-site, which are experimentally difficult to achieve. The creation of supersolid-like regions by introducing a superlattice is experimentally straight-forward, however. Similar to the ordinary supersolid, the supersolid-like regions considered here are also only stable for relatively small hopping, while for larger hopping the "ordinary" superfluid behavior dominates as we will see below.

As long as the hopping t is sufficiently small the alternation of anisotropies between Mott and SD phases continues as the density is increased due to the same reasoning as above. However, this is not the full story since for larger hopping t or larger filling \bar{n} the Mott and SD phases are not stable, so it is not clear where the different regions of positive and negative ρ_-^s are separated. Indeed as shown in Fig. 4, the superfluid density does not drop to zero for $\bar{n} = 4/3$ and $\Delta\mu/U = 0.25$, since the corresponding line is just outside the lobe of the SD-2 phase as shown in Fig. 3(b). Also the anisotropy no longer changes sign. We find that in the limit of large hopping t the overall density becomes irrelevant. The sublattice A remains slightly more occupied for all values of \bar{n} and t .

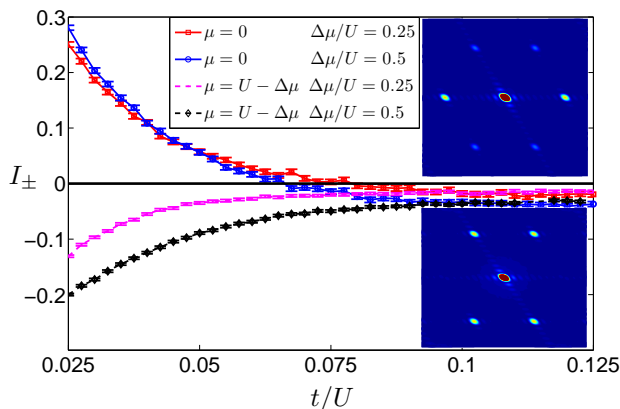


FIG. 5: Superfluid anisotropy parameter $I_{\pm} = (\rho_1^s - \rho_2^s)/(\rho_1^s + \rho_2^s)$ as a function of t/U from QMC for $\beta U = 2000$ and $N = 432$ in the parameter range indicated by the horizontal lines in Fig. 3. Insets: QMC simulations of the TOF image for $t/U = 0.0375$, $\beta U = 800$, $N = 243$, $\Delta\mu/U = 0.5$, and $\mu/U = -0.175$ (top) and $\mu/U = 0.425$ (bottom).

Since particles on the A sublattice hardly hop in the \vec{a}_1 direction, this leads to $\rho_1^s < \rho_2^s$ in the weak coupling limit $t > U$. We call this behavior the "ordinary" superfluid, in contrast to the supersolid-like regions of the positive anisotropy $\rho_-^s > 0$, which are basically confined between the lobes of the SD-n and Mott-n phases.

To analyze the crossover between different anisotropy regions we show the normalized anisotropy parameter $I_{\pm} = (\rho_1^s - \rho_2^s)/(\rho_1^s + \rho_2^s)$ as a function of t/U for different values μ and $\Delta\mu$ in Fig. 5. For small hopping the anisotropy parameter I_{\pm} is positive in supersolid-like regions ($\mu = 0$) and negative between the Mott-1 and SD-2 phase ($\mu = U - \Delta\mu$) as discussed above. For larger t/U the anisotropy parameters approach small negative values in all cases, corresponding to the ordinary superfluid. According to the analysis above, the sign-change of I_{\pm} as a function of t coincides with the delocalization of the particles on the A sublattice, which start to contribute to the superfluid density in the \vec{a}_2 direction. This behavior can be interpreted as a continuous "melting" of the supersolid-like phase to the ordinary superfluid, reminiscent of the melting of the sublattice order in an interaction driven supersolid [33].

Anisotropic superfluid densities appear in a variety of different systems such as dipolar Bose-Einstein condensates with disorder [43–45], spin-orbit coupled Fermi gases [46], coupled spin dimer systems [47], and systems with rectangular shape [48]. However, an anisotropic superfluidity which is tunable by the isotropic hopping t and changes sign when the order on one sublattice melts has not been discussed before to our knowledge.

The observation of the superfluid-Mott transition by time-of-flight (TOF) experiments has been pioneered many years ago [6]. The TOF absorption picture measures the momentum distribution $S(\mathbf{Q})/N =$

$(|\sum_{k=1}^N a_k^{\dagger} e^{i\mathbf{Q}\cdot\mathbf{r}_k}|^2)/N^2$ and turns out to also show a clear signature of the anisotropy parameter. To demonstrate this effect, we used a QMC technique for calculating the off-diagonal long-range correlation function during the loop update [49], which allows a direct simulation of the TOF absorption signal. As shown in Fig. 5 for $\rho_-^s > 0$ (upper inset) and for $\rho_-^s < 0$ (lower inset) the TOF images display a clear signature of the anisotropy, which can be used for straight-forward measurements of the melting from supersolid-like to ordinary superfluid states.

In conclusion, we analyzed ultracold bosons in a kagome superlattice, which can be created and tuned by enhancing the long wavelength laser in one direction based on recent progress for creating highly frustrated lattices [21]. By using numerical QMC simulations and the Generalized Effective Potential Landau Theory, we obtained the entire quantum phase diagram including Mott phases and fractionally filled charge density phases. In the superfluid phase an anisotropic superfluid density is found, which changes direction as the overall density or the hopping is changed. By tuning the hopping it is possible to induce a continuous *melting* from a supersolid-like state with a filled sublattice A and positive anisotropy parameter $\rho_-^s > 0$ to an ordinary superfluid phase, which generically is characterized by a negative anisotropy parameter $\rho_-^s < 0$. Both the fractionally filled insulating phases and supersolid phases have received much attention by using models with longer-range interactions [29–35]. Using the superlattice structure proposed in this work these phases become experimentally much more accessible by a simple laser setup instead of using dipolar interactions. Moreover, the characteristic signature of those effects can be measured in straight-forward TOF absorption experiments, without the need of single site resolution. In particular, by implementing off-diagonal measurements in QMC loop updates, it was possible to simulate TOF flight images which show a clear signature of the anisotropic superfluid density and the change of its direction, when the melting takes place.

X.-F. Zhang thanks for discussions with D. Morath about TOF calculations and with Y.C. Wen about superlattices. This work was supported by the Allianz für Hochleistungsrechnen Rheinland-Pfalz and by the German Research Foundation (DFG) via the Collaborative Research Center SFB/TR49.

* Electronic address: axel.pelster@physik.uni-kl.de

- [1] R. P. Feynman, Int. J. Theor. Phys. **21**, 467 (1982).
- [2] I. Bloch, J. Dalibard, and W. Zwerger, Rev. Mod. Phys. **80**, 885 (2008).
- [3] I. Bloch, J. Dalibard, and S. Nascimbène, Nat. Phys. **8**, 267 (2012).
- [4] M. Lewenstein, A. Sanpera, and V. Ahufinger, *Ultracold*

- Atoms in Optical Lattices: Simulating Quantum Many-Body Systems* (Oxford University Press, Oxford, 2012).
- [5] A. Vogler, *et. al.*, Phys. Rev. Lett. **113**, 215301 (2014).
- [6] M. Greiner, O. Mandel, T. Esslinger, T.W. Hänsch, and I. Bloch, Nature **415**, 39 (2002).
- [7] M.P.A. Fisher, P.B. Weichman, G. Grinstein, and D.S. Fisher, Phys. Rev. B **40**, 546 (1989).
- [8] D. Jaksch, C. Bruder, J. I. Cirac, C. W. Gardiner, and P. Zoller, Phys. Rev. Lett. **81**, 3108 (1998).
- [9] A. Micheli, G. K. Brennen, and P. Zoller, Nat. Phys. **2**, 341 (2006).
- [10] S. Peil, J. V. Porto, B. L. Tolra, J. M. Obrecht, B. E. King, M. Subbotin, S. L. Rolston, and W. D. Phillips, Phys. Rev. A **67**, 051603(R) (2003).
- [11] J. Sebby-Strabley, M. Anderlini, P. S. Jessen, and J. V. Porto, Phys. Rev. A **73**, 033605 (2006).
- [12] S. Fölling, S. Trotzky, P. Cheinet, M. Feld, R. Saers, A. Widera, T. Müller, and I. Bloch, Nature **448**, 1029 (2007).
- [13] P. Cheinet, S. Trotzky, M. Feld, U. Schnorrberger, M. Moreno-Cardoner, S. Fölling, and I. Bloch, Phys. Rev. Lett. **101**, 090404 (2008).
- [14] P. Buonsante and A. Vezzani, Phys. Rev. A **70**, 033608 (2004).
- [15] B.-L. Chen, S.-P. Kou, Y. Zhang, and S. Chen, Phys. Rev. A **81**, 053608 (2010).
- [16] A. Dhar, T. Mishra, R. V. Pai, and B. P. Das, Phys. Rev. A **83**, 053621 (2011).
- [17] A. Dhar, M. Singh, R. V. Pai, and B. P. Das, Phys. Rev. A **84**, 033631 (2011).
- [18] T. Wang, X.-F. Zhang, S. Eggert, A. Pelster, Phys. Rev. A **87**, 063615 (2013).
- [19] P. Windpassinger and K. Sengstock, Rep. Prog. Phys. **76**, 086401 (2013).
- [20] J. Struck, C. Ölschlager, R. Le Targat, P. Soltan-Panahi, A. Eckardt, M. Lewenstein, P. Windpassinger, and K. Sengstock, Science **333**, 996 (2011).
- [21] G.-B. Jo, J. Guzman, C. K. Thomas, P. Hosur, A. Vishwanath and D. M. Stamper-Kurn, Phys. Rev. Lett. **108**, 045305 (2012).
- [22] X.-G. Wen, *Quantum Field Theory of Many-Body Systems* (Oxford University Press, Oxford, 2004).
- [23] G. Evenbly and G. Vidal, Phys. Rev. Lett. **104**, 187203 (2010).
- [24] S. Yan, D. A. Huse and S. R. White, Science **332**, 1173 (2011).
- [25] T.-H. Han, J. S. Helton, S. Y. Chu, D. G. Nocera, J. A. Rodriguez-Rivera, C. Broholm, and Y. S. Lee, Nature **492**, 406 (2012).
- [26] Y. Iqbal, F. Becca, S. Sorella, and D. Poilblanc, Phys. Rev. B **87**, 060405(R) (2013).
- [27] S. Capponi, V. R. Chandra, A. Auerbach, and M. Weinstein, Phys. Rev. B **87**, 161118(R) (2013).
- [28] H. O. Jeschke, F. Salvat-Pujol, and R. Valenti, Phys. Rev. B **88**, 075106 (2013).
- [29] S. V. Isakov, S. Wessel, R. G. Melko, K. Sengupta, and Y. B. Kim, Phys. Rev. Lett. **97**, 147202 (2006).
- [30] A. O'Brien, F. Pollmann, and P. Fulde, Phys. Rev. B **81**, 235115 (2010).
- [31] L.F. Tocchio, C. Gros, X.-F. Zhang, and S. Eggert, Phys. Rev. Lett. **113**, 246405 (2014).
- [32] X.-F. Zhang and S. Eggert, Phys. Rev. Lett. **111**, 147201 (2013).
- [33] X.-F. Zhang, R. Dillenschneider, Y. Yu, and S. Eggert, Phys. Rev. B **84**, 174515 (2011).
- [34] L. Bonnes and S. Wessel, Phys. Rev. B **84**, 054510 (2011).
- [35] D. Yamamoto, I. Danshita, and C. A. R. Sá de Melo, Phys. Rev. A **85**, 021601(R) (2012).
- [36] D. Sellmann, X.-F. Zhang, and S. Eggert, Phys. Rev. B **91**, 081104(R) (2015).
- [37] A. W. Sandvik, Phys. Rev. B **59**, 14157(R) (1999).
- [38] O. F. Syljuåsen and A. W. Sandvik, Phys. Rev. E **66**, 046701 (2002).
- [39] K. Louis and C. Gros, Phys. Rev. B **70**, 100410(R) (2004).
- [40] F.E.A. dos Santos and A. Pelster, Phys. Rev. A **79**, 013614 (2009).
- [41] E. L. Pollock and D. M. Ceperley Phys. Rev. B **36**, 8343 (1987).
- [42] M. Ueda, *Fundamentals and New Frontiers of Bose-Einstein Condensation* (World Scientific, Singapore, 2010).
- [43] C. Krumnow and A. Pelster, Phys. Rev. A **84**, 021608(R) (2011).
- [44] B. Nikolic, A. Balaz, and A. Pelster, Phys. Rev. A **88**, 013624 (2013).
- [45] M. Ghabour and A. Pelster, Phys. Rev. A **90**, 063636 (2014).
- [46] J. P.A. Devreese, J. Tempere, and C. A.R. Sa de Melo, Phys. Rev. Lett. **113**, 165304 (2014).
- [47] D. Straßel, P. Kopietz, and S. Eggert Phys. Rev. B **91**, 134406 (2015).
- [48] R. G. Melko, A. W. Sandvik, and D. J. Scalapino Phys. Rev. B **69**, 014509 (2004).
- [49] A. Dorneich and M. Troyer Phys. Rev. E **64**, 066701 (2001).